Submitted for publication in ApJ
Preprint typeset using LaTeX style emulateapj v. 01/23/15

UNCERTAINTY ON THE GALAXY-HALO CONNECTION FOR LYMAN-α EMITTERS AT $Z = 3.1$

Julián E. Mejía-Restrepo [1,3], Jaime E. Forero-Romero [2]
[1]Departamento de Astronomía, Universidad de Chile, Camino el Observatorio 1515, Santiago, Chile
[2]Departamento de Física, Universidad de los Andes, Cra. 1 No. 18A-10, Edificio Ip, Bogotá, Colombia
[3]FACom-Instituto de Física-FCEN, Universidad de Antioquia, Calle 70 No. 52-21, Medellín, Colombia
Submitted for publication in ApJ

ABSTRACT

We study the impact of cosmic variance and observational uncertainties in constraining the mass and occupation fraction, $f_{\rm occ}$, of dark matter halos hosting Lyα Emitting Galaxies (LAEs) at high redshift. We construct mock catalogs from an N-body simulation to match the typical size of observed fields at $z = 3.1$ ($\sim 1{\rm deg}^2$). In our model a dark matter halo with mass in the range $M_{\rm min} < M_{\rm h} < M_{\rm max}$ can only host one detectable LAEat most. We explore the parameter space determined by $M_{\rm min}$, $M_{\rm max}$ and $f_{\rm occ}$ with a Markov Chain Monte-Carlo algorithm using as observational constraints the angular correlation function (ACF) and the LAEs number density. We find that the preferred minium and maximum masses in our model span a wide range $10^{9.8}h^{-1}{\rm M}_\odot \leq M_{\rm min} \leq 10^{11.0}h^{-1}{\rm M}_\odot$, $10^{10.9}h^{-1}{\rm M}_\odot \leq M_{\rm max} \leq 10^{13.0}h^{-1}{\rm M}_\odot$; followed by a wide range in the occupation fraction $0.02 \leq f_{\rm occ} \leq 0.30$. As a consequence the median mass, M_{50}, of all models consistent with observations has a large uncertainty $M_{50} = 3.16^{+9.34}_{-2.37} \times 10^{10}h^{-1}{\rm M}_\odot$. However, we find that the same individual models have a relatively tight 1σ mass gap $\Delta M_{1\sigma} = 0.55^{+0.11}_{-0.31}$ dex. We are also able show that $f_{\rm occ}$ is uniquely determined by $M_{\rm min}$, regardless of $M_{\rm max}$. We argue that upcoming large surveys covering at least 25 deg^2 should be able to put tighter constraints on $M_{\rm min}$ and $f_{\rm occ}$ through the LAE number density distribution width, $W_{1\sigma}$, constructed over several fields of ~ 1 deg^2.

Subject headings: Galaxies: halos — Galaxies: high-redshift — Galaxies: statistics — Dark Matter — Methods: numerical

1. INTRODUCTION

Lyman-α emitting galaxies (LAEs) are central to a wide range of subjects in extragalactic astronomy. LAEs can be used as probes of reionization (for a recent review see Dijkstra 2014, and references therein), tracers of large scale structure (Koehler et al. 2007), signposts for low metallicity stellar populations (for a recent review see Hayes 2015, and references therein), markers of the galaxy formation process at high redshift (Partridge & Peebles 1967; Rhoads et al. 2000; Blanc et al. 2011) and tracers of active star formation.

In most of those cases, capitalizing the observations requires understanding how LAEs are formed within an explicit cosmological context. Under the current structure formation paradigm the dominant matter content of the Universe is dark matter (DM). Each galaxy is thought to be hosted by a larger dark matter structure known as a halo. (Peebles 1980; Springel et al. 2005). Understanding the cosmological context of LAEs thus implies studying the galaxy-halo connection. Galaxy formation models suggest that the physical processes that regulate the star formation cycle are dependent on halo mass (e.g. Behroozi et al. 2013). The mass becomes the most important element in the halo-galaxy connection.

The goal becomes finding the typical DM halo mass of halos hosting LAEs. In the case of LAEs there are different ways to find this mass range. One approach is theoretical, using general astrophysical principles to find the relationship between halo mass, intrinsic Lyα luminosities and observed Lyα luminosities. This approach is usually implemented through semi-analytic models (Garel et al. 2012; Orsi et al. 2012) and full N-body hydrodynamical simulations (Laursen & Sommer-Larsen 2007; Dayal et al. 2009; Forero-Romero et al. 2011; Yajima et al. 2012).

The downside of these calculations is the uncertainty in the estimation of the escape fraction of Lyα photons. Given the resonant nature of the Lyα line, the escape fraction is sensitive to the dust contents, density, temperature, topology and kinematics of the neutral Hydrogen in the interstellar medium (ISM). The process of finding a consensus on the expected value for the Lyα escape fraction in high redshift galaxies is still matter of open debate (Neufeld 1991; Verhamme et al. 2006; Forero-Romero et al. 2012; Dijkstra & Kramer 2012; Laursen et al. 2013; Orsi et al. 2012; Yajima et al. 2014).

A different approach to infer the typical mass of halos hosting LAEs is based on the spatial clustering information. This approach uses the fact that in CDM cosmologies the spatial clustering of galaxies on large scales is entirely dictated by the halo distribution (Colberg et al. 2000), which in turn has a strong dependence on halo mass. Using measurements of the angular correlation function of LAEs, observers have put constraints on the typical mass and occupation fraction of the putative halos hosting these galaxies (Hayashino et al. 2004; Gawiser et al. 2007b; Nilsson et al. 2007; Ouchi et al. 2010; Bielby et al. 2016). In these studies the observations are done on fields of ~ 1 deg^2 and the conclusions derived on the halo host mass do not elaborate on the uncertainty resulting from the cosmic variance on these fields.

In this letter we investigate the impact of cosmic variance in constraining the mass and occupation fraction of halos hosting LAEs at $z = 3$. We build mock surveys from a cosmological N-body simulation to compare them

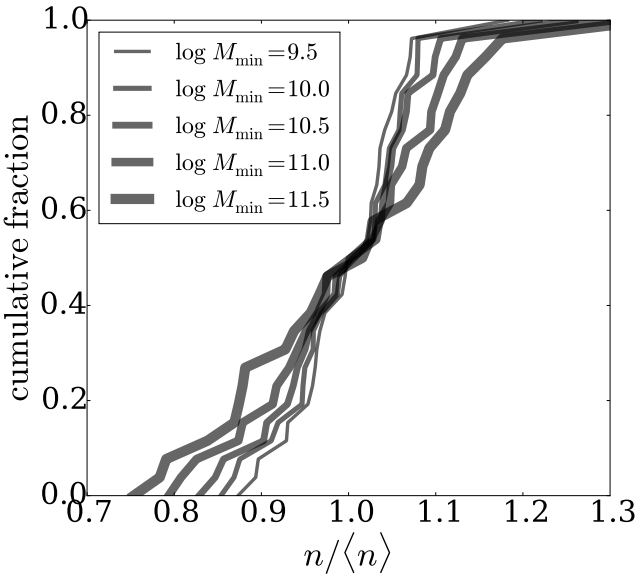

FIG. 1.— Cumulative halo number density distribution function over 27 mock fields. Each line corresponds to a different model with increasig values of $M_{\rm min}$. Different models produce different number density distributions. The width of the distribution increases with $M_{\rm min}$.

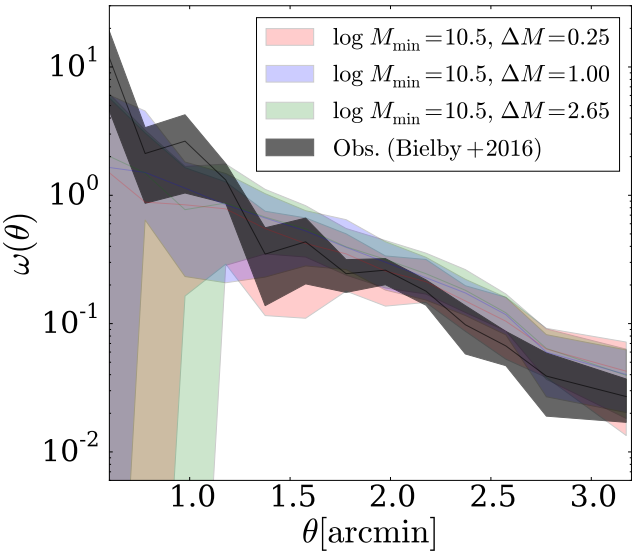

FIG. 2.— Angular Correlation functions for $\log M_{\rm min}[{\rm M}_\odot {\rm h}^{-1}] = 10.5$ and different values of $\Delta \log M$. The shaded region in the models represents the $1-\sigma$ variation due to cosmic variance. Radically different models in $\Delta \log M$ are consistent with observations once cosmic variance is modelled in detail.

against the observations of Bielby et al. (2016) using the angular correlation function. We use a simple model to populate a halo in the simulation with a LAE assuming a minimum, $M_{\rm min}$, and maximum mass, $M_{\rm max}$, for the dark matter halos hosting LAEs without assuming an underlying relation between the Lyα luminosity and the dark matter halo mass. This approach bypasses all the physical uncertainties associated to star formation and radiative transfer. We then use the Markov Chain Monte Carlo technique to obtain the likelihood of the parameters given the observational constraints.

Throughout this letter we assume a ΛCDM cosmology with the following values for the cosmological parameters, $\Omega_m = 0.30711$, $\Omega_\Lambda = 0.69289$ and $h = 0.70$, corresponding to the matter density, vacuum density and the Hubble constant in units of 100 km s^{-1} Mpc^{-1}.

2. METHODOLOGY

The base of our method is the comparison between observations and mock catalogs. This approach allows us to take explicitly into account cosmic variance. The comparison has four key elements. First, the observations we take as a benchmark. Second, the N-body simulation and the halo catalogs we use to build the mocks. Third, the parameters describing our model to assign a LAE to a halo. Fourth, the statistical method we adopt to compare observations and simulations. We describe in detail these four elements in the following subsections.

2.1. *Observational constraints*

Bielby et al. (2016) used narrow band imaging to detect 643 LAE candidates at $z \sim 3$ with Ly-α equivalent widths of $\gtrsim$65Å and a Ly-α flux limit of 2×10^{17}erg/cm^2/s ($L \sim 7 \times 10^{42}$erg/s). Using spectroscopy they found a 22% contamination fraction $f_{\rm c}$. Their observations cover 5 (out of 9) independent and adjacent fields of the VLT LBG Redshift Survey (VLRS). The total observed area corresponds to 1.07deg^2 that translates to $\sim 80^2 h^{-1}$Mpc^2 in a comoving scale. Bielby et al. (2016) used the NB497 narrow-band filter whose 77Å FWHM and 154Å Full width tenth maximum (FWTM) correspond to a total observational depth of $44h^{-1}$Mpc and $82h^{-1}$Mpc comoving, respectively.

2.2. *Simulation and halo catalog*

We use results from the BolshoiP simulation (Klypin et al. 2011, 2014) performed in a cubic volume of 250 h^{-1} Mpc comoving on a side. The dark matter distribution was sampled using 2048^3 particles. The cosmological parameters are consistent with Planck results (Planck Collaboration et al. 2014) with a matter density $\Omega_{\rm m} = 0.307$, cosmological constant $\Omega_\Lambda = 0.693$, dimensionless Hubble constant $h = 0.678$, slope of the power spectrum $n = 0.96$ and normalization of the power spectrum $\sigma_8 = 0.823$. This translates into a particle mass of $m_{\rm p} = 1.5 \times 10^8$ h^{-1} M$_\odot$.

We use halo catalogs constructed with a Bound-Density-Maxima (BDM) algorithm. The catalogs were obtained from the publicly available Multidark database [1] (Riebe et al. 2013). For each halo in the box we extract its comoving position and mass. We focus our work on halos more massive than $1.5 \times 10^9 h^{-1}$M$_\odot$ resolved with at least 40 particles to guarantee a well behaved halo mass function. We do not take into account sub-halos.

We split the simulation volume at z∼3 into 27 smaller mock volumes mimicking the area and depth reported in Bielby et al. (2016) and described in §2.1.

2.3. *A simple LAE model*

We build the simplest possible model to assign a LAE to each DM halo without trying to compute a LAE luminosity.

We first assume that a dark matter halo can host one detectable LAE at most. This assumption is consistent

[1] http://www.multidark.org/MultiDark/

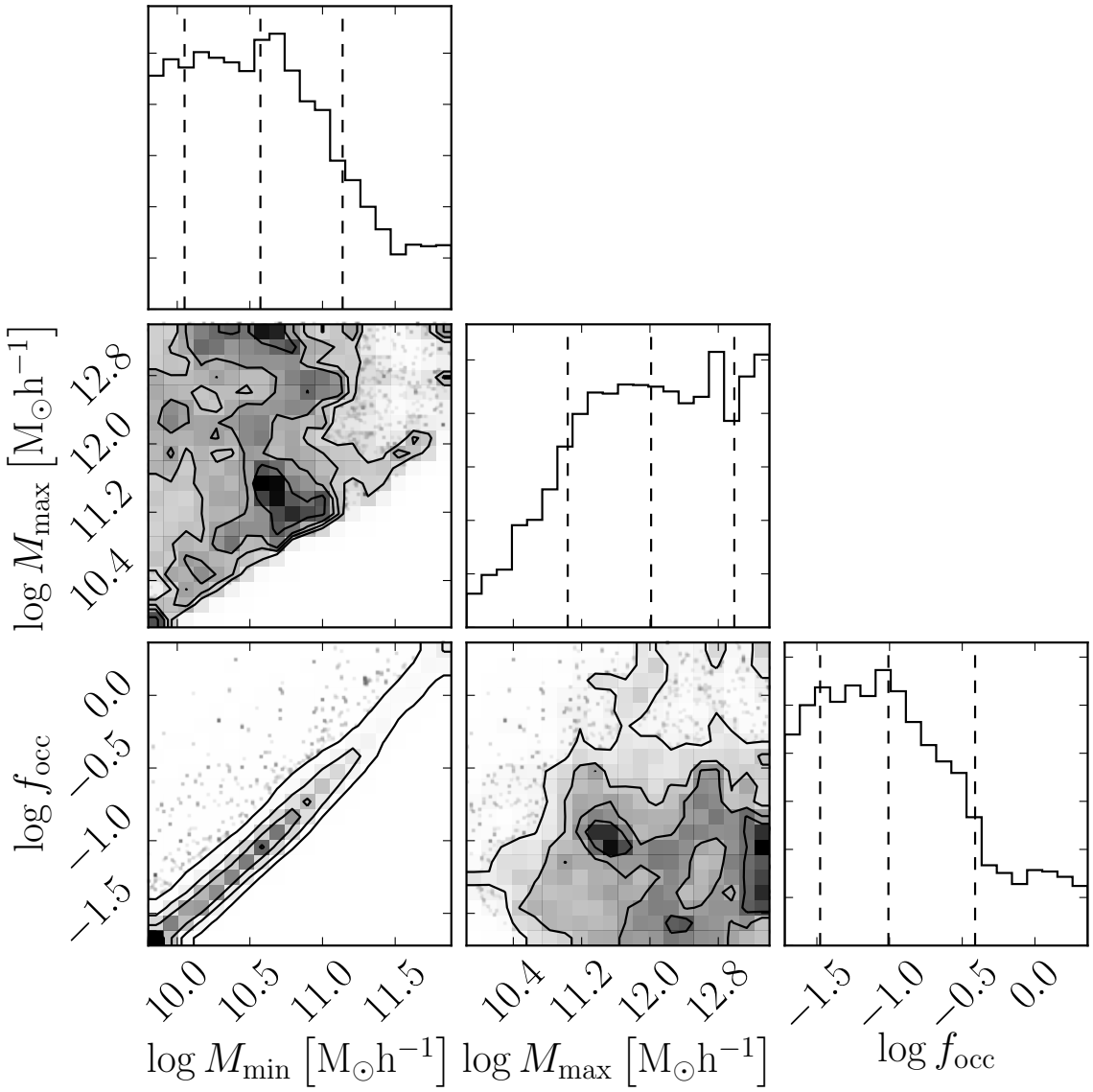

FIG. 3.— One and two dimensional projections of the posterior probability distributions of $M_{\rm min}$, $M_{\rm max}$ and $f_{\rm occ}$.The models with $\log f_{\rm occ} > 0.00$ ($f_{\rm occ} > 1$) correspond to models where the number density of halos is smaller than the number of observed LAEs but we consider them as consistent because of the uncertainty in the median number density due to cosmic variance. See Fig. 1 and §2.4 for details.

with theoretical analysis of the correlation function (Jose et al. 2013) and observations that confirm a lack of class pairs in LAEs Bond et al. (2009). Then we say that a halo will host a LAE with probability $f_{\rm occ}$ if and only if the halo mass is in the range $M_{\rm min} < M_{\rm h} < M_{\rm max}$. We also use the variable $\Delta \log M$to represent the mass range width, $\Delta \log M \equiv \log M_{\rm max} - \log M_{\rm max}$.

An astrophysical interpretation of $f_{\rm occ}$ convolves at least four phenomena: the actual presence of a star forming galaxy in a halo, a duty cycle in the star formation rate, the escape fraction of Lyα radiation and its detectability as a LAE with Ly-α equivalent widths of $\gtrsim$65Å. We do not try to disentangle these effects and do not assume an underlying relation between the α luminosity and the dark matter halo mass. We instead opt for a purely arithmetic interpretation by setting $f_{\rm occ}$ as the ratio between the observed number of LAEs and the number of halos within the considered mass range, that is $f_{\rm occ} \equiv N_{\rm LAEs}/N_{\rm halos}$.

For each mock catalog we also randomly remove a fraction $f_{\rm c} = 0.22$ of the mock-LAEs and replace them with randomly distrubuted points to mimic the effect of interloper contamination in Bielby et al. (2016) observations. On top of that we apply rejection sampling to our LAE selection along the radial direction taking the transmission function of the NB479 filter used in Bielby et al. (2016) observations.

Fig. 1 shows the cumulative halo number density for all 27 subvolumes in the simulation, with a normalization by the average number density among fields. Each line represents a different model $\mathcal{M}$ with fixed $f_{\rm occ} = 1$ and $\Delta \log M = 1.0$; and varying $M_{\rm min}$, This Figure shows that the halo number density varies across sub-volumes, as an expression of cosmic variance. As a consequence,

the $f_{\rm occ}$ also varies across the mock fields by the same factor factor.

In what follows we note by the letter $\mathcal{M}$ a model defined by a particular choice of the two parameters $M_{\rm min}$, $M_{\rm max}$. For each model $\mathcal{M}$ we define $\tilde{f}_{\rm occ}$ as the median occupation fraction within the the mock fields.

2.4. *Model Selection*

We explore the parameter space of the models $\mathcal{M}$ by means of the Affine Invariant Markov Chain Monte Carlo technique using the EMCEE python package (Foreman-Mackey et al. 2013, and references therein).

The MCMC exploration is done using a total of 24 seeds and 400 iterations (9600 models) to sample the posterior probability distribution function ($P(\mathcal{M}|\text{observations})$ based on the Angular Correlation Function (ACF). We put a flat prior on $\log M_{\rm min}$ and $\log M_{\rm max}$ between 9.8 up to 13.4, corresponding to the halo mass range of the simulation at $z = 3$. We restrict the selection to models that give a minimal number density $N_{\rm halos} > N_{\rm LAE}/3$. This means that it is possible to have $N_{\rm halos} < N_{\rm LAE}$ and hence $f_{\rm occ} \equiv N_{\rm LAE}/N_{\rm halos} > 1$. We include the 1/3 factor to account for the uncertainty in the number density of LAEs due to cosmic variance, expecting it to be on the same order as the dark matter halo cosmic variance shown in Fig. 1. Our likelihood is taken proportional to $\exp(-\chi^2_{\mathcal{M}}/2)$, with the $\chi^2_{\mathcal{M}}$ where:

$$\chi^2_{\mathcal{M}} = \sum_{\theta} \left[\frac{\left(\mathrm{ACF}_{\mathcal{M}}(\theta) - \mathrm{ACF}_{\rm obs}(\theta)\right)^2}{\sigma^2_{\mathcal{M}}(\theta) + \sigma^2_{\rm obs}(\theta)} \right] \qquad (1)$$

Here $\mathrm{ACF}_{\mathcal{M}}$ and $\mathrm{ACF}_{\rm obs}$ are the ACF of the explored model $\mathcal{M}$ and the observational ACF reported by Bielby et al. (2016) respectively. $\sigma_{\mathcal{M}}$ is the associated 1-σ scatter of the $\mathrm{ACF}_{\mathcal{M}}$ as a product of cosmic variance and $\sigma_{\rm obs}$ is the observational error associated to $\mathrm{ACF}_{\rm obs}$.

We compute the $\mathrm{ACF}_{\mathcal{M}}$ using the Landy & Szalay estimator (Landy & Szalay 1993). After this, we correct the computed ACF from the contamination fraction of interlopers $f_{\rm c}$ multiplying the ACF by a factor of $1/(1-f_{\rm c})^2$ following the procedure described in Bielby et al. (2016).

Fig. 2 shows the observational ACF by Bielby et al. (2016) compared to the ACF in three different models with a wide range in $\Delta \log M$. This already shows that radically different models can be compatible with observations once cosmic variance uncertainties are modelled in detail.

3. RESULTS AND DISCUSSION

3.1. *Constraints on Model Parameters*

Fig. 3 shows the one and two dimensional projections of the posterior probability distributions of the parameters in our LAE model. This Figure represents our main result: $M_{\rm min}$, $M_{\rm max}$ and $f_{\rm occ}$ cannot be tightly constrained from the available observations.

The preferred $1-\sigma$ range for the masses is $9.6 < \log M_{\rm min} < 11.0$ and $10.9 < \log M_{\rm max} < 13.0$. $f_{\rm occ}$ is completely determined by $M_{\rm min}$ from $f_{\rm occ}$=0.015 when $\log M_{\rm min} = 9.6$ to $f_{\rm occ} = 0.30$ when $\log M_{\rm min} = 11.0$. We compute the power-law dependece between $f_{\rm occ}$ and $M_{\rm min}$ to be

$$f_{\rm occ} = 0.1 \left(\frac{M_{\rm min}}{10^{10.5} h^{-1} \mathrm{M}_\odot} \right)^{0.93}. \qquad (2)$$

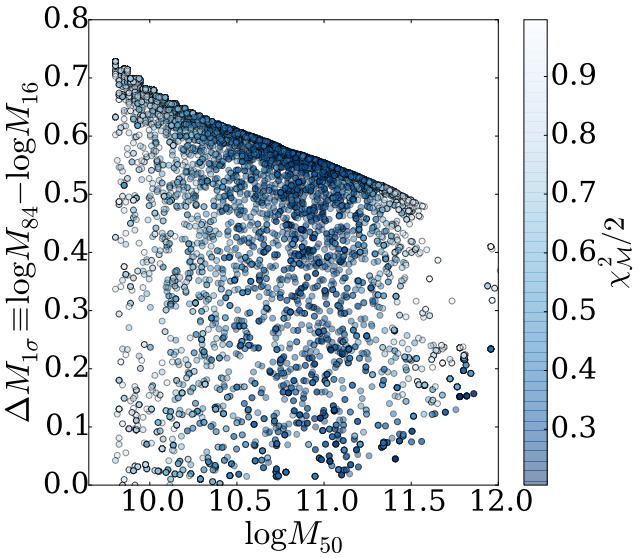

FIG. 4.— Median mass, $\log M_{50}$, and mass width $\Delta \log M_{1\sigma} = \log M_{84} - \log M_{16}$, for all models with low $\chi^2_{\mathcal{M}}/2 < 1.0$. The median mass spans two orders of magnitude with a mean value around $10^{10.5} h^{-1}\mathrm{M}_\odot$. The mass width $\Delta \log M_{1\sigma}$ has a median of 0.55 dex (a factor of ~ 3 in mass) with a maximum value of 0.7 dex (a factor of 5). This means that all models consistent with observations have a very narrow range in halo mass.

We remind the reader that models whith $\log f_{\rm occ} > 0.00$ ($f_{\rm occ} > 1$) correspond to cases where the halo number density is smaller than the number of observed LAEs but are still considered consistent because of the expected uncertainty in the median number density of LAEs due to cosmic variance (see Fig. 1 and §2.4).

3.2. *Median Halo Mass and Halo Mass Width within Models*

We now compute the median mass, $\log M_{50}$, and the 1σ halo mass width, $\Delta \log M_{1\sigma} \equiv \log M_{84} - \log M_{16}$, of the LAE hosting halos for each model $\mathcal{M}$ (here M_p represents the p percentile of the mass distribution); $\log M_{50}$ and $M_{1\sigma}$ allow a direct comparison between our results and previous results in the literature (e.g. Hayashino et al. 2004; Gawiser et al. 2007a; Ouchi et al. 2010; Bielby et al. 2016) that used a more simplified semi-analitical approach.

In Fig. 4 we show the $\log M_{50}$-$\Delta \log M_{1\sigma}$ plane for the models selected to have $\chi^2_{\mathcal{M}}/2 < 1$, which roughly correspond to the 1σ region in the posterior distribution for the model parameters. The color encodes the $\chi^2_{\mathcal{M}}/2$ value. The median mass has a wide distribution spanning two orders of magnitude.

From this distribution we obtain $\log M_{50} = 10.5 \pm 0.6$ or equivalently $M_{50} = 3.16^{+9.34}_{-2.37} \times 10^{10} h^{-1}\mathrm{M}_\odot$. The 1σ uncertainty for this median value is estimated from the 16 and 84 percentile values in the $\log M_{50}$ distribution.

Our result is consistent within the statistical uncertainties with previous estimates reported by Bielby et al. (2016) ($\tilde{M}_{\rm h} = 10^{11.0 \pm 0.6} h^{-1}\mathrm{M}_\odot$), Gawiser et al. (2007b) ($\tilde{M}_{\rm h} = 10^{10.9 \pm 0.9} h^{-1}\mathrm{M}_\odot$) and Ouchi et al. (2010) ($\tilde{M}_{\rm h} = 10^{10.8^{+1.8}_{-0.8}} h^{-1}\mathrm{M}_\odot$) using semi-analitical approaches. In spite of the large uncertainties, we note that our median mass is systematically below theirs by 0.3 to 0.5 dex.

However, the same Figure 4 shows something that semi-analytical approaches were not able to predict. The

mass width, $\Delta \log M_{1\sigma}$, that is the width of the mass distribution for a given model with fixed $M_{\rm min}$ and $M_{\rm max}$, has a median value and 1σ uncertainty of $\Delta \log M_{1\sigma} = 0.55^{+0.11}_{-0.31}$ dex. This means that the mass range for halos hosting LAEs is very narrow. There is only a factor of 2 to 4 between the lower and upper mass boundary of the central 68 percentile of the mass distribution. We emphasize that $M_{\rm max}$ can still be very large while the width is small due to the asymetry in the dark matter halo mass function.

Summarizing, the median mass could be anything in the range $10^{9.5} h^{-1}{\rm M}_\odot$ and $10^{11.5} h^{-1}{\rm M}_\odot$ (a 2.0 dex range), but the 1-σ width of the mass distribution is highly constrained to be between 0.2 and 0.6 dex.

In Fig. 2 we show the computed $ACF_{\mathcal{M}}$ of models with $\log M_{\rm min} = 10.5$ and different values of $\Delta \log M$. We can see that the clustering gets slightly stronger for larger values of $\Delta \log M$. Nevertheless, due to the large impact of cosmic variance at the volume of the current observations all the models are basically consistent within errors. The last result together with the large Poissonian observational error in the ACF explain the current difficulty to put tighter constrains in $\log M_{\rm max}$ in our model.

3.3. *Constraining Dark matter halos mass with cosmic variance*

Fig. 1 shows the halo number distribution (HND) in the mock fields of the simulation for different models $\mathcal{M}$. By simple inspection one can infer that the distribution width increases with $M_{\rm min}$.

In Fig. 5 we confirm this trend by plotting the HND 1σ width for good models ($\chi^2_{\mathcal{M}}/2 < 1$) as a function of $\log M_{\rm min}$. We find that considering all the mock 25 field the 1σ width, $W_{1\sigma}$ increases with $M_{\rm min}$following

$$W_{1\sigma} = (0.138 \pm 0.002) \times \left(\frac{M_{\rm min}}{10^{11} h^{-1}{\rm M}_\odot} \right)^{0.177 \pm 0.009} . \quad (3)$$

This result opens the possibility to constrain the $\log M_{\rm min}$(as well as the median mass) of LAEs by simply measuring the width of the distribution of observed LAE along several observational fields. This idea has been already explored for $z > 6$ galaxies (Robertson 2010).

To keep the validity of Eq. (3) there should at least be 27 fields (to follow the same numbers we use here) of size $\sim$ 1deg^2 with the same observational coditions (filters, equivalent width cuts). However, repeating the same kind of cosmic variance study for different survey strategies should help to provide a constraint of the same kind.

4. CONCLUSIONS

In this letter we studied the impact of cosmic variance and observational uncertainties in constraining the mass range and occupation fraction of dark matter halos hosting LAEs. To this end we used the BolshoiP N-body simulation to construct 27 mock fields with the same typical size of observed fields at $z = 3.1$ ($\sim$ 1deg^2). In our model a dark matter halo with mass in the range $M_{\rm min} < M_h < M_{\rm max}$ can only host one detectable LAE at most. We explored the parameter space determined by $M_{\rm min}$ and $M_{\rm max}$ using Monte Carlo Markov-Chain minimization to match the observed ACF and mean number density of LAEs. It is the first time that such a thorough exploration of the cosmic variance impact on LAEs statistics is presented in the literature.

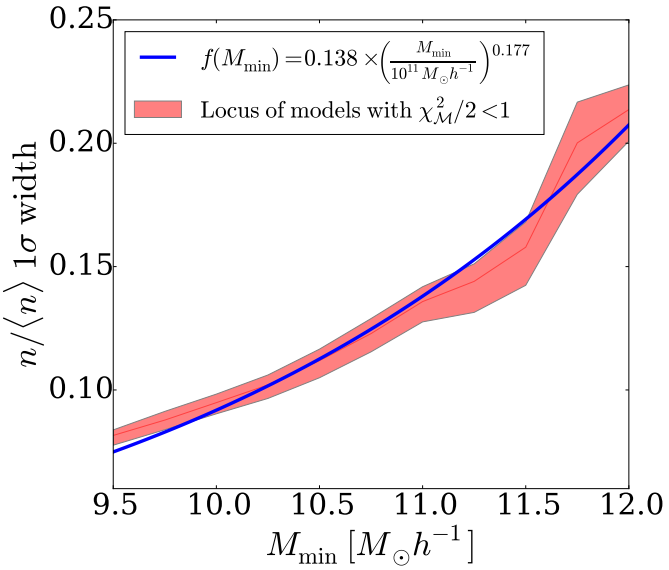

FIG. 5.— 1σ width of the number density distribution over the 54 mock fields of the simulation as a function of $M_{\rm min}$. Only the models that have a good match with observations ($\chi_{\mathcal{M}}/2 < 1$) are included. The strong dependence of $n/\langle n \rangle$ with $M_{\rm min}$was parameterized as a power law with the parameters shown in the legend.

We find that once cosmic variance is taken into account, the observational data can only put weak constraints on $M_{\rm max}$ and $f_{\rm occ}$. When we translate these loos constraints into the median mass, we find a general consistency with previous works (Hayashino et al. 2004; Gawiser et al. 2007b; Ouchi et al. 2008) specially with the most recent one (Bielby et al. 2016).

Nevertheless, our analysis allowed us to draw two results that can be used to put tighter constraints on $M_{\rm min}$and $f_{\rm occ}$once upcoming large LAE surveys, such as the HETDEX project (Adams et al. 2011) and the HSC ultra deep survey, are available:

1. $f_{\rm occ}$is uniquely determined by $M_{\rm min}$, regardless of $M_{\rm max}$. A precise determination of $M_{\rm min}$ will thus fix $f_{\rm occ}$. As a consequence of this, for a given $M_{\rm min}$the media mass is also fixed.

2. The width of the LAE number distribution function obtained over several fields of $\approx$ 1 deg^2 is tightly correlated with $M_{\rm min}$. That measurement with next generation surveys will be able to constrain $M_{\rm min}$within a factor of $\sim$ 2.

We also find that the 1-σ width of the mass distribution is highly constrained to be between 0.2 and 0.6 dex. This result can be used to test different models for LAEs formation in a cosmological context to better understand why observable LAEs are constrained into a narrow halo mass range.

ACKNOWLEDGMENTS

JEMR acknowledges "CONICYT-PCHA/doctorado Nacional para extranjeros/2013-63130316" for their PhD scholarship support.

JEFR acknowledges financial support from Vicerrectoría de Investigaciones at Uniandes from a a FAPA project.

The authors gratefully acknowledge the Gauss Centre for Supercomputing e.V. (www.gauss-centre.eu) and the Partnership for Advanced Supercomputing in Europe (PRACE, www.prace-ri.eu) for funding the MultiDark simulation project by providing computing time on the GCS Supercomputer SuperMUC at Leibniz Supercomputing Centre (LRZ, www.lrz.de). The Bolshoi simulations have been performed within the Bolshoi project of the University of California High-Performance AstroComputing Center (UC-HiPACC) and were run at the NASA Ames Research Center.

REFERENCES

Adams, J. J., Blanc, G. A., Hill, G. J., Gebhardt, K., Drory, N., Hao, L., Bender, R., Byun, J., Ciardullo, R., Cornell, M. E., Finkelstein, S. L., Fry, A., Gawiser, E., Gronwall, C., Hopp, U., Jeong, D., Kelz, A., Kelzenberg, R., Komatsu, E., MacQueen, P. J., Murphy, J., Odoms, P. S., Roth, M., Schneider, D. P., Tufts, J. R., & Wilkinson, C. P. 2011, ApJS, 192, 5

Behroozi, P. S., Wechsler, R. H., & Conroy, C. 2013, ApJ, 770, 57

Bielby, R. M., Tummuangpak, P., Shanks, T., Francke, H., Crighton, N. H. M., Bañados, E., González-López, J., Infante, L., & Orsi, A. 2016, MNRAS, 456, 4061

Blanc, G. A., Adams, J. J., Gebhardt, K., Hill, G. J., Drory, N., Hao, L., Bender, R., Ciardullo, R., Finkelstein, S. L., Fry, A. B., Gawiser, E., Gronwall, C., Hopp, U., Jeong, D., Kelzenberg, R., Komatsu, E., MacQueen, P., Murphy, J. D., Roth, M. M., Schneider, D. P., & Tufts, J. 2011, ApJ, 736, 31

Bond, N. A., Gawiser, E., Gronwall, C., Ciardullo, R., Altmann, M., & Schawinski, K. 2009, ApJ, 705, 639

Colberg, J. M., White, S. D. M., Yoshida, N., MacFarland, T. J., Jenkins, A., Frenk, C. S., Pearce, F. R., Evrard, A. E., Couchman, H. M. P., Efstathiou, G., Peacock, J. A., Thomas, P. A., & Virgo Consortium. 2000, MNRAS, 319, 209

Dayal, P., Ferrara, A., Saro, A., Salvaterra, R., Borgani, S., & Tornatore, L. 2009, MNRAS, 400, 2000

Dijkstra, M. 2014, PASA, 31, e040

Dijkstra, M., & Kramer, R. 2012, MNRAS, 424, 1672

Foreman-Mackey, D., Hogg, D. W., Lang, D., & Goodman, J. 2013, PASP, 125, 306

Forero-Romero, J. E., Yepes, G., Gottlöber, S., Knollmann, S. R., Cuesta, A. J., & Prada, F. 2011, MNRAS, 415, 3666

Forero-Romero, J. E., Yepes, G., Gottlöber, S., & Prada, F. 2012, MNRAS, 419, 952

Garel, T., Blaizot, J., Guiderdoni, B., Schaerer, D., Verhamme, A., & Hayes, M. 2012, MNRAS, 422, 310

Gawiser, E., Francke, H., Lai, K., Schawinski, K., Gronwall, C., Ciardullo, R., Quadri, R., Orsi, A., Barrientos, L. F., Blanc, G. A., Fazio, G., & Feldmeier, J. J. 2007a, ApJ, 671, 278

Gawiser, E., Francke, H., Lai, K., Schawinski, K., Gronwall, C., Ciardullo, R., Quadri, R., Orsi, A., Barrientos, L. F., Blanc, G. A., Fazio, G., Feldmeier, J. J., Huang, J.-s., Infante, L., Lira, P., & Padilla, N. 2007b, ApJ, 671, 278

Hayashino, T., Matsuda, Y., Tamura, H., Yamauchi, R., Yamada, T., Ajiki, M., Fujita, S. S., Murayama, T., Nagao, T., Ohta, K., Okamura, S., Ouchi, M., Shimasaku, K., Shioya, Y., & Taniguchi, Y. 2004, AJ, 128, 2073

Hayes, M. 2015, PASA, 32, e027

Jose, C., Srianand, R., & Subramanian, K. 2013, ArXiv e-prints

Klypin, A., Yepes, G., Gottlober, S., Prada, F., & Hess, S. 2014, ArXiv e-prints

Klypin, A. A., Trujillo-Gomez, S., & Primack, J. 2011, ApJ, 740, 102

Koehler, R. S., Schuecker, P., & Gebhardt, K. 2007, A&A, 462, 7

Landy, S. D., & Szalay, A. S. 1993, ApJ, 412, 64

Laursen, P., Duval, F., & Östlin, G. 2013, ApJ, 766, 124

Laursen, P., & Sommer-Larsen, J. 2007, ApJ, 657, L69

Neufeld, D. A. 1991, ApJ, 370, L85

Nilsson, K. K., Møller, P., Möller, O., Fynbo, J. P. U., Michałowski, M. J., Watson, D., Ledoux, C., Rosati, P., Pedersen, K., & Grove, L. F. 2007, A&A, 471, 71

Orsi, A., Lacey, C. G., & Baugh, C. M. 2012, MNRAS, 425, 87

Ouchi, M., Shimasaku, K., Akiyama, M., Simpson, C., Saito, T., Ueda, Y., Furusawa, H., Sekiguchi, K., Yamada, T., Kodama, T., Kashikawa, N., Okamura, S., Iye, M., Takata, T., Yoshida, M., & Yoshida, M. 2008, ApJS, 176, 301

Ouchi, M., Shimasaku, K., Furusawa, H., Saito, T., Yoshida, M., Akiyama, M., Ono, Y., Yamada, T., Ota, K., Kashikawa, N., Iye, M., Kodama, T., Okamura, S., Simpson, C., & Yoshida, M. 2010, ApJ, 723, 869

Partridge, R. B., & Peebles, P. J. E. 1967, ApJ, 147, 868

Peebles, P. J. E. 1980, The large-scale structure of the universe

Planck Collaboration, Ade, P. A. R., Aghanim, N., Armitage-Caplan, C., Arnaud, M., Ashdown, M., Atrio-Barandela, F., Aumont, J., Baccigalupi, C., Banday, A. J., & et al. 2014, A&A, 571, A16

Rhoads, J. E., Malhotra, S., Dey, A., Stern, D., Spinrad, H., & Jannuzi, B. T. 2000, ApJ, 545, L85

Riebe, K., Partl, A. M., Enke, H., Forero-Romero, J., Gottlber, S., Klypin, A., Lemson, G., Prada, F., Primack, J. R., Steinmetz, M., & Turchaninov, V. 2013, Astronomische Nachrichten, 334, 691

Robertson, B. E. 2010, ApJ, 716, L229

Springel, V., White, S. D. M., Jenkins, A., Frenk, C. S., Yoshida, N., Gao, L., Navarro, J., Thacker, R., Croton, D., Helly, J., Peacock, J. A., Cole, S., Thomas, P., Couchman, H., Evrard, A., Colberg, J., & Pearce, F. 2005, Nature, 435, 629

Verhamme, A., Schaerer, D., & Maselli, A. 2006, A&A, 460, 397

Yajima, H., Choi, J.-H., & Nagamine, K. 2012, MNRAS, 427, 2889

Yajima, H., Li, Y., Zhu, Q., Abel, T., Gronwall, C., & Ciardullo, R. 2014, MNRAS, 440, 776